

Scale effects in the post-cracking behaviour of fibre-reinforced concrete beams

*Original*

Scale effects in the post-cracking behaviour of fibre-reinforced concrete beams / Carpinteri, A.; Accornero, F.; Rubino, A.. - In: INTERNATIONAL JOURNAL OF FRACTURE. - ISSN 0376-9429. - ELETTRONICO. - 240:(2023), pp. 1-16. [10.1007/s10704-022-00671-x]

*Availability:*

This version is available at: 11583/2975502 since: 2023-02-01T15:45:48Z

*Publisher:*

Springer

*Published*

DOI:10.1007/s10704-022-00671-x

*Terms of use:*

This article is made available under terms and conditions as specified in the corresponding bibliographic description in the repository

*Publisher copyright*

(Article begins on next page)



# Scale effects in the post-cracking behaviour of fibre-reinforced concrete beams

Alberto Carpinteri · Federico Accornero · Alessio Rubino

Received: 29 March 2022 / Accepted: 23 September 2022 / Published online: 3 November 2022  
© The Author(s) 2022

**Abstract** The scale effects on the global structural response of fibre-reinforced concrete (FRC) beams subjected to bending are discussed in the framework of Fracture Mechanics by means of the Updated Bridged Crack Model (UBCM). This model predicts different post-cracking regimes depending on two dimensionless numbers: the *reinforcement brittleness number*,  $N_p$ , which is related to the fibre volume fraction,  $V_f$ ; and the *pull-out brittleness number*,  $N_w$ , which is related to the fibre embedment length,  $w_c$ . Both these dimensionless numbers depend on the beam depth,  $h$ , which, keeping the other variables to be constant, drives a ductile-to-brittle transition in the post-cracking regime of the composite. The critical value of the reinforcement brittleness number,  $N_{PC}$ , allows for prediction of the minimum (critical) specimen size,  $h_{min}$ , which, analogously to the minimum fibre volume fraction,  $V_{f,min}$ , is required to achieve a stable post-cracking response. Numerical simulations are compared to experimental results reported in the scientific literature, in which FRC specimens, characterized by the same fibre volume fraction but different sizes, are tested in bending.

**Keywords** Fibre-reinforced concrete · Updated Bridged Crack Model · Post-cracking regimes · Scale effects · Minimum reinforcement condition

## 1 Introduction

During the last decades, extensive research, both theoretical and experimental, was carried out in order to investigate the different parameters affecting the cracking behaviour of fibre-reinforced concrete (FRC) structural elements.

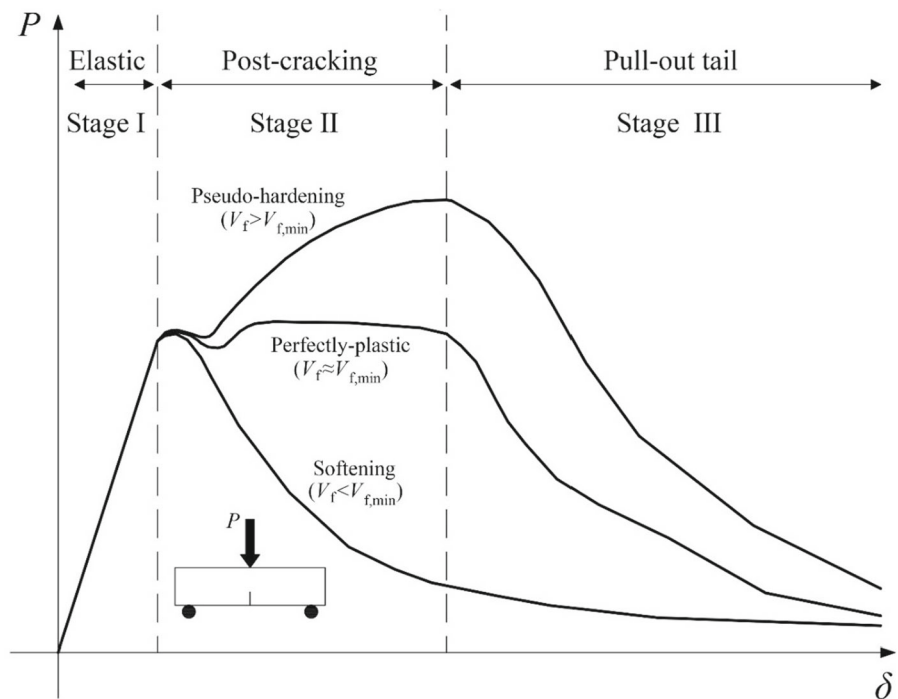
Considering a FRC beam subjected to bending, several experimental studies suggest describing the flexural response, usually represented in terms of the applied load vs deflection diagram, by sub-dividing it into three different stages (Fig. 1). The structural behaviour starts with a linear ascending branch (Stage I), until the onset of the fracturing process. From this point onwards, the post-cracking regime (Stage II) takes place, which depends, among other parameters, on the fibre volume fraction,  $V_f$ . A deflection-softening or deflection-hardening behaviour can be observed, leading to the definition of the so-called minimum (or critical) fibre volume fraction,  $V_{f,min}$ , which is required to guarantee a stable post-cracking branch. The latter occurs when the maximum load experienced by the specimen, i.e., the load bearing capacity, is equal to or greater than the applied load at the onset of crack

---

A. Carpinteri · F. Accornero (✉) · A. Rubino  
Department of Structural, Geotechnical and Building  
Engineering, Politecnico di Torino, Turin, Italy  
e-mail: federico.accornero@polito.it

A. Carpinteri  
Department of Civil and Environmental Engineering,  
Shantou University, Shantou, People's Republic of China

**Fig. 1** Typical experimental load vs deflection curves of FRC beams



propagation. On the contrary, if the fibre volume content is not sufficiently high, i.e.,  $V_f < V_{f,min}$ , this intermediate stage may not develop. Finally, the flexural response is described by a descending tail (Stage III) of the load vs deflection curve, which represents the fibre pull-out or rupture.

In this framework, different experimental investigations carried out so far indicate that the flexural performance of FRC specimens is affected by: (i) the fibre volume fraction,  $V_f$  (Almusallam et al. 2016; Barr et al. 2003; Barros and Sena Cruz 2001; Barros et al. 2005; Bencardino et al. 2010; Fantilli et al. 2016; Holschemacher et al. 2010; Mobasher et al. 2014; Naaman 2008; Soetens and Matthys 2014); (ii) the mechanical and geometrical properties of the reinforcing fibres (tensile strength, geometric profile, and aspect ratio) and of the cementitious matrix (Aydin 2013; Choi et al. 2019; Sahin and Koksal 2011; Yoo et al. 2015); (iii) the specimen size (Flàdr and Bily 2018; Jones et al. 2008; Paschalis and Lampropoulos 2015; Yoo et al. 2016).

In the latter case, recent experimental studies show a systematic decrease in the composite flexural strength—calculated with an elastic approach—by increasing the specimen size (Flàdr and Bily 2018; Paschalis and Lampropoulos 2015; Yoo et al. 2016).

This geometric effect, which can be also related to the fibre distribution within the volume of the composite (Lo Monte and Ferrara 2020), can be quantitatively evaluated in the framework of Fracture Mechanics by using the Multi-fractal Scaling Law (MFSL) for initially uncracked specimens (Carpinteri 1994), or the Size Effect Law (SEL) for initially cracked specimens (Bažant 1984). These best-fitting laws were extensively discussed in the case of quasi-brittle materials.

The scale effects are also taken into account in the latest RILEM Recommendations (RILEM TC 162-TDF 2003) for the design of FRC structures, where the residual flexural stresses (evaluated at a specific crack mouth opening displacement, CMOD) are adjusted by a coefficient, which decreases with the increase in the specimen size.

In the present paper, size effects on the global post-cracking behaviour of FRC beams are investigated in the framework of Fracture Mechanics by means of the Updated Bridged Crack Model (UBCM). This model, originally proposed for steel-bar reinforced concrete elements (Carpinteri 1981, 1984a, b), has been adapted by some of the authors to the case of brittle-matrix fibrous composites subjected to bending (Bosco and Carpinteri 1995; Carpinteri and Massabò

1996, 1997a, b; Carpinteri and Puzzi 2007; Carpinteri and Accornero 2019, 2020). More recently, further applications of the model to the case of FRC beams have been discussed in Accornero et al. (2020, 2022a, b) and Rubino et al. (2021). In this work, the focus is on the scale-dependent post-cracking regimes predicted by the model, as a function of two dimensionless numbers,  $N_P$  and  $N_w$ . Moreover, the critical value of the reinforcement brittleness number,  $N_{PC}$ , allows for prediction of the minimum (critical) fibre volume fraction (Rubino et al. 2021),  $V_{f,min}$ , or, equivalently, the critical specimen size,  $h_{min}$ , required to guarantee a stable post-cracking response. In the following sections, the main features of the model will be recalled, and the related numerical predictions will be validated on the basis of experimental data reported in the scientific literature.

## 2 The Updated Bridged Crack Model (UBCM)

Considering a FRC beam element subjected to flexural loading, the model is able to describe the evolution of the fracturing process occurring in a notched rectangular cross-section where the damage is localized. The cross-section is characterized by the thickness,  $b$ , the depth,  $h$ , the initial edge crack depth,  $a_0$ , and it is subjected to an external bending moment,  $M$  (Fig. 2).

On the left of Fig. 3, a schematic of the notched cross-section subjected to bending is reported. Experimental evidences lead to identify the following four regions: (i) ligament in compression; (ii) uncracked ligament in tension; (iii) fibre bridging zone, in which

the reinforcing fibres bridge the crack; (iv) stress-free crack zone—generally noticeable for large crack depths or very short fibres—where the bridging action of the fibres has vanished.

These regions can be effectively interpreted in the UBCM. The model assumes the composite as a bi-phase material, in which the brittle matrix and the reinforcing fibres represent its primary and secondary phase, both contributing to the global toughness. The matrix is assumed to be linear elastic, being neglected other nonlinear contributions (nonlinear tensile and compression behaviours). In agreement with Linear Elastic Fracture Mechanics (LEFM), a singular stress distribution is predicted at the crack tip (see the right part of Fig. 3), and the matrix toughening contribution is defined by its fracture toughness,  $K_{IC}$ .

On the other hand, the bridging mechanism of the secondary phase can be described by an appropriate cohesive softening constitutive law, which takes into account the progressive slippage of the fibre inside the matrix. The corresponding toughening contribution relates to the energy required to pull-out a single fibre and it is predominant if compared to that of the matrix.

In the framework of UBCM, the bridging action of the reinforcing fibres can be modelled by means of a discontinuous (discrete) formulation or a continuous one, which have been discussed in Carpinteri and Massabò (1997a). In the present investigation, the discontinuous version of the model is taken into account, for which the reinforcing fibres are considered as discrete entities. This assumption requires the following information: (i) the number of fibres in the critical cross-section under investigation; (ii) the

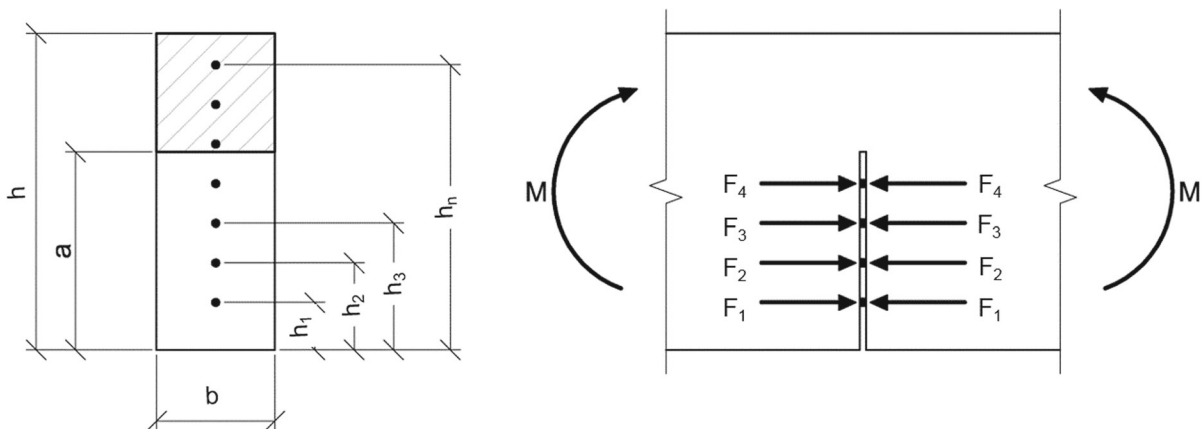


**Fig. 2** Fibre-reinforced brittle-matrix beam model

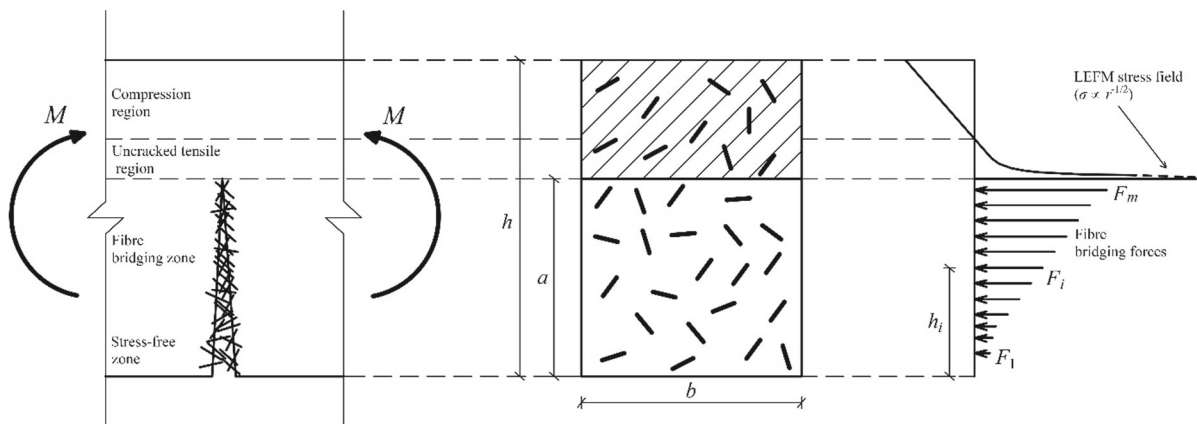


**Fig. 3** Critical cross-section of FRC beams with the stress distribution predicted by the UBCM

position of the fibres; (iii) the bridging force of each fibre.

The total number of fibres in the cross-section,  $n$ , can be calculated as  $n = \alpha V_f b h / A_f$ , where  $A_f$  is the cross-sectional area of the single fibre, and  $\alpha$  the orientation factor. The coefficient  $\alpha$  is defined as the ratio of the actual number of fibres in the critical section—obtained by investigating the specimen fracture surface—to the theoretical one (Robins et al. 2003).

Regarding the fibre position, they are considered evenly spaced in the ligament area, each one characterized by the corresponding level arm,  $h_i$ , measured with respect to the bottom edge of the beam (see Fig. 2 and the right part of Fig. 3). The model disregards other factors that can affect the actual distribution of the fibres in the specimen volume, such as the casting procedure, wall effect, etc.

The  $m < n$  fibres crossing the actual crack are considered as active and their bridging action is taken into account by the closure forces,  $F_i$ , calculated as  $F_i = \beta_i \sigma_s A_f$ , in which  $\sigma_s$  is the nominal stress of the  $i$ -th reinforcing fibres adjusted by a coefficient  $\beta_i$ . The latter is useful to define an equivalent stress acting in the fibre, which includes other phenomena as the “group effect” (the maximum pull-out force per fibre decreases as the number of fibres increases) and the “snubbing effect” (the maximum pull-out force changes due to the fibre orientation with respect to the applied load) (Li et al. 1990). The influence of these two parameters related to the fibre distribution,  $\alpha$  and  $\beta$ , will be discussed later in the paper.

Under these assumptions, the singular crack-tip stress field is uniquely characterized by a global stress-intensity factor,  $K_I$ :

$$K_I = K_{IM} - \sum_{i=1}^m K_{Ii} = \frac{M}{bh^{3/2}} Y_M - \frac{\{Y_F\}^T \{F\}}{bh^{1/2}}, \quad (1)$$

in which the contributions related to the applied bending moment,  $K_{IM}$ , and to the  $i$ -th reinforcing fibre,  $K_{Ii}$ , appear. In agreement with the LEFM criterion, the crack propagation occurs when the stress-intensity factor,  $K_I$ , reaches its critical value,  $K_{IC}$ , i.e. the fracture toughness of the plain matrix (unreinforced material).

The bridging forces provided by the  $m$  active reinforcing layers can be calculated by means of a cohesive softening constitutive law, which takes into account the slippage mechanism of the fibres from the cementitious matrix. The latter is typically investigated by means of pull-out tests carried out on the single fibre. Namely, the pull-out response of a short fibre in a cementitious matrix depends on several factors, among which the fibre material (steel, polypropylene, natural, etc.), the fibre geometry (straight, crimped, twisted, with hooked ends, etc.), the orientation of the fibre with respect to the pull-out load, and the fibre embedment length (Abdallah et al. 2018).

In the following, the pull-out laws are defined for steel fibres characterized by straight or hooked-end profiles. In addition, the fibre is considered as aligned with respect to the applied load, and slippage is the main bridging mechanism. The fibre rupture, which usually occurs in the case of high orientation angle

(Robins et al. 2002), or high-strength matrices coupled with low resistance fibres (Aydin 2013; Choi et al. 2019; Sahin and Koksal 2011; Yoo et al. 2015), is here excluded.

Under these assumptions, the pull-out response of a straight fibre is characterized by an initial ascending branch in which the bonding mechanism is due to the chemical adhesion between the fibre and the surrounding concrete. When the fibre is completely debonded and the pull-out strength is reached, the response is governed by the frictional mechanism, leading to a decrease in the slippage load until the fibre is entirely pulled-out from the matrix (Abdallah et al. 2018).

On the other hand, the pull-out response of an hooked-end steel fibre is characterized by an intermediate stage which reflects the mechanical interlocking of the fibre hooks. With respect to a straight fibre, this additional mechanism leads to an increase in the maximum pull-out load and to a variation in the shape of the constitutive law, which is now characterized by two horizontal plastic plateaux corresponding to the hook straightening (Alwan et al. 1999).

Therefore, two different constitutive laws have been implemented in UBCM (Fig. 4). In both cases, the constitutive law is defined by two parameters: (i) the slippage strength of the fibre,  $\sigma_{s,max}$ , beyond which the fibre pull-out starts; (ii) the fibre embedment length,  $w_c$ , beyond which the fibre bridging action is exhausted. The area subtended by the bridging laws represents the contribution of the reinforcing fibres to the global toughness of the composite.

Considering the experimental investigation reported in the literature, a power-law (Fig. 5a;  $n = 0.5$ ) seems appropriate to describe the pull-out behaviour of straight steel fibres. On the other hand, a piecewise function, indicated as  $f$  in Fig. 4b, has been recently suggested in the case of hooked-end steel fibres (Abdallah and Rees 2019). The analytical expressions of these constitutive laws can be found in Accornero et al. (2022a), in which the effectiveness of UBCM in reproducing the flexural response of FRC members is discussed.

Finally, a set of compatibility conditions is introduced to calculate the crack opening,  $w_i$ , at each  $i$ -th active reinforcement level as a function of the applied bending moment,  $M$ , and of the  $m$  bridging forces,  $F_i$ . In matrix form:

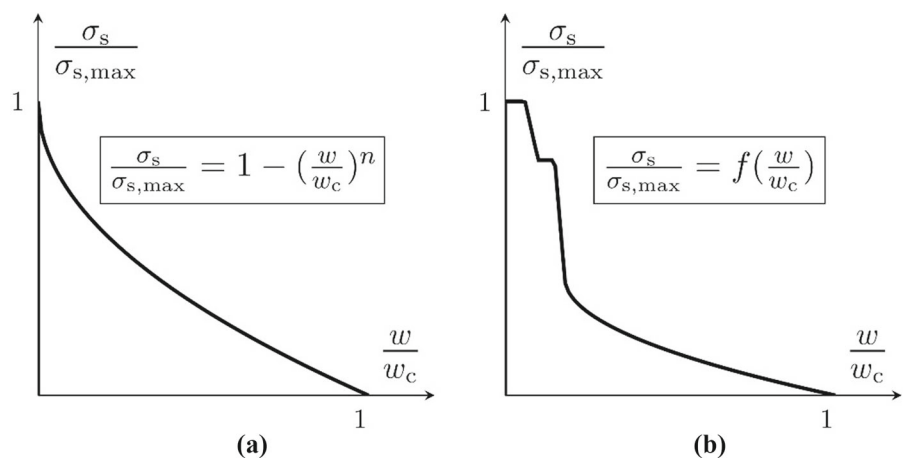
$$\{w\} = \{\lambda_M\}M - [\lambda]\{F\}, \tag{2}$$

where  $\{w\}$  is the crack opening vector,  $\{\lambda_M\}$  is the vector of the local compliances due to the bending moment, and  $[\lambda]$  is the matrix of the local compliances due to the bridging forces.

Summarizing, for a given crack depth, the problem relies in the determination of the  $2m + 1$  unknowns, i.e., the fracturing moment,  $M_F$ , the profile of the crack opening displacements,  $\{w\}$ , and the corresponding distribution of bridging forces,  $\{F\}$ . The solution requires a numerical iterative procedure that leads to the complete evaluation of the stress-block diagram as schematically represented in Fig. 3.

At each loading step, i.e., for each crack length, the local rotation of the notched cross-section can be calculated as:

**Fig. 4** Slippage law per unit embedded length: **a** straight fibre; **b** hooked-end fibre



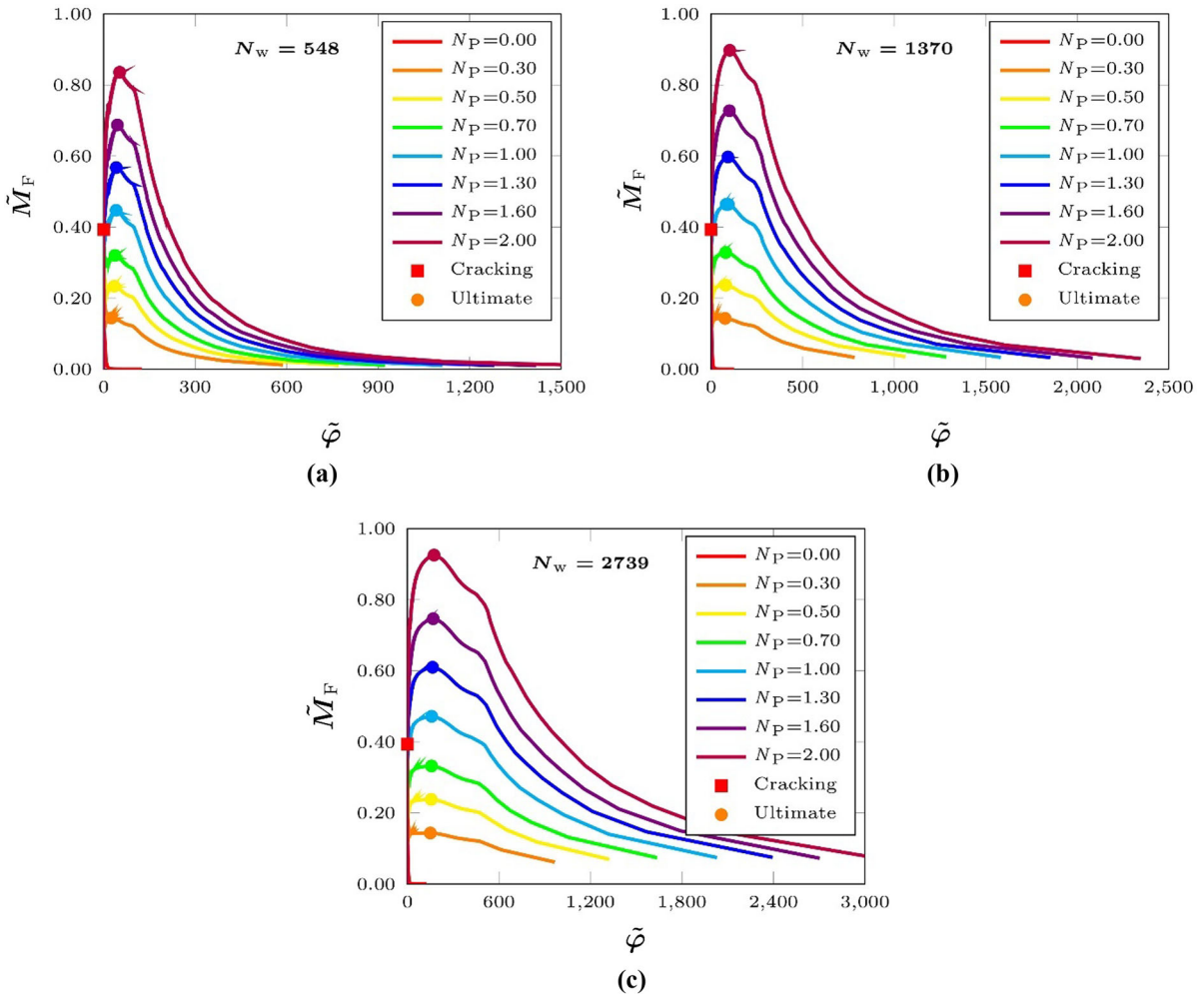


**Fig. 5** Structural response of FRC beams ( $a_0/h = 0.05$ ) as a function of  $N_p$ , and for different values of  $N_w$ : **a**  $N_w = 548$ ; **b**  $N_w = 1370$ ; **c**  $N_w = 2739$ . For each curve, the square marker

indicates the first cracking moment, whereas the circle one indicates the ultimate moment

$$\varphi = \lambda_{MM}M - \{\lambda_M\}^T\{F\}. \tag{3}$$

The corresponding deflection of the FRC element,  $\delta$ , can be obtained by applying the superposition principle, according to which the total deflection takes into account both the inelastic contribution related to the fracturing process in the mid-span section (inelastic hinge) and that related to the elastic behaviour of the remaining part of the beam.

Under these assumptions, the UBCM is able to predict the FRC different post-cracking regimes ranging from softening to pseudo-hardening (Fig. 1) as a function of two scale-dependent dimensionless numbers, i.e., the *reinforcement brittleness number*,  $N_p$ , and the *pull-out brittleness number*,  $N_w$ :

$$N_p = \frac{\sum_{i=1}^n F_{P,i}}{K_{IC}bh^{1/2}} = V_f \frac{\alpha\bar{\beta}\sigma_{s,max}}{K_{IC}} h^{1/2} = V_f \frac{\bar{\sigma}_{s,max}}{K_{IC}} h^{1/2}, \tag{4}$$

$$N_w = \frac{Ew_c}{K_{IC}h^{1/2}}. \tag{5}$$

The reinforcement brittleness number,  $N_p$ , represents the dimensionless maximum value of the bridging forces. It depends on the fibre volume fraction,  $V_f$ , on the maximum value of the generalized slippage strength of the fibre,  $\bar{\sigma}_{s,max}$ —in which the parameters of fibre distribution,  $\alpha$  and  $\beta$  are included—on the matrix fracture toughness,  $K_{IC}$ , as well as on the beam depth,  $h$ . On the other hand,  $N_w$  depends on the matrix

Young's modulus,  $E$ , on the fibre embedment length,  $w_c$ , on the matrix fracture toughness,  $K_{IC}$ , and on the beam depth,  $h$ .

In Eq. (4),  $\tilde{\sigma}_{s,max}$ , is obtained as the product between the orientation factor,  $\alpha$ , the average value of the coefficients  $\beta_i$  (it is different for each fibre),  $\bar{\beta}$ , and the slippage strength of the fibre,  $\sigma_{s,max}$ . In this sense, it is worth emphasizing that  $\tilde{\sigma}_{s,max}$  englobes the information related to the actual distribution and orientation of the fibres in the critical cross-section. As a consequence, the analysis of the FRC structural response does not require the determination of the single values  $\alpha$  and  $\bar{\beta}$ , but only of  $\tilde{\sigma}_{s,max}$ , which can be identified on the basis of experimental flexural tests.

In addition, it is worth noting that the product between  $N_P$  and  $N_w$ , which is equal to  $V_f \tilde{\sigma}_{s,max} w_c E / K_{IC}^2$ , provides an information regarding the toughening contribution of the two constituent phases of the composite. As a matter of fact, it is proportional to the ratio between the toughening contribution provided by the reinforcing secondary phase, which is calculated as the area subtended by the bridging traction law (Fig. 4), and the fracture energy of the brittle concrete matrix, which is calculated as a function of  $K_{IC}$  by means of the Irwin's relationship. This product is used to thoroughly describe the post-cracking structural behaviours of brittle-matrix fibrous composites (Masabò 2008).

### 3 Numerical simulations

Let us consider a FRC cross-section characterized by a notch depth equal to 1/20 of the beam depth ( $a_0/h = 0.05$ ), and reinforced with hooked-end steel fibres (Fig. 4b). The critical cross-section is characterised by a discrete number of reinforcing layers,  $n = 100$ , which are considered to be evenly spaced in the ligament area and orthogonal with respect to the crack faces. In this sense, the coefficients  $\alpha$  and  $\beta_i$  have been assumed equal to 1. By means of the UBCM, the structural responses are plotted by varying the fibre volume fraction,  $V_f$ , and the fibre embedment length,  $w_c$ , in order to highlight the influence of  $N_P$  and  $N_w$  on the post-cracking behaviour of the FRC beams.

In Fig. 5a–c, three sets of numerical curves are represented, each of them referring to a constant value

of  $N_w$ , whereas  $N_P$  ranges from 0 (unreinforced material) to 2.

The three stages previously described (Fig. 1) can be clearly identified in each numerical curve. The elastic branch—valid until the first cracking moment (red square marker) is reached ( $\tilde{M}_{cr} = 0.39$  for  $a_0/h = 0.05$ )—is the same for all the curves. When the crack starts propagating, the response is characterized by an intermediate stage (Stage II), in which the ultimate bending moment of the cross-section,  $\tilde{M}_u$ , is defined (circle markers). Depending on  $N_P$ , the post-cracking response could be unstable, when the ultimate moment is smaller than the first cracking moment (see red, orange, yellow, and green curves), or stable, when the ultimate moment is greater than the first cracking moment (see cyan, blue, violet, and purple curves). This suggests to define the critical value of the reinforcement brittleness number,  $N_{PC}$  ( $= 0.83$  for  $a_0/h = 0.05$ ), which is required to guarantee a stable post-cracking response (ultimate bending moment equal to the first cracking moment) (Accornero et al. 2022). In all cases, a decrement in the load is observed in the final stage of the response (Stage III), which is governed by  $N_w$ . The latter, when sufficiently small (see Fig. 5a), provides the convergence of all the curves to a unique final softening branch.

Similar conclusions can be drawn in the case of the numerical simulations represented in Fig. 6a–c. In this case, each of the three families of curves corresponds to a constant value of  $N_P$ , whereas  $N_w$  ranges from 274 to 2739. Consistent with the previous considerations, the stability of the post-cracking response in the Stage II—ranging from softening (Fig. 6a) to pseudo-hardening (Fig. 6c)—is defined by  $N_P$ . Then, for a given value of  $N_P$ , the numerical curves slip towards different final softening branches depending on the value of  $N_w$ , which has small influence on the ultimate bending moment, although it defines the rotational capacity at the cross-sectional level. The rotational capacity is intended as the difference between the local rotation occurring at the ultimate bending moment (circle marker) and the local rotation related to the first cracking moment (square marker).

It is worth noting that these transitions in the flexural response hold even if a different value of the initial notch depth,  $a_0/h$ , is assumed. This parameter affects the initial elastic branch of the response (Stage I), thus leading to a different value of the first cracking



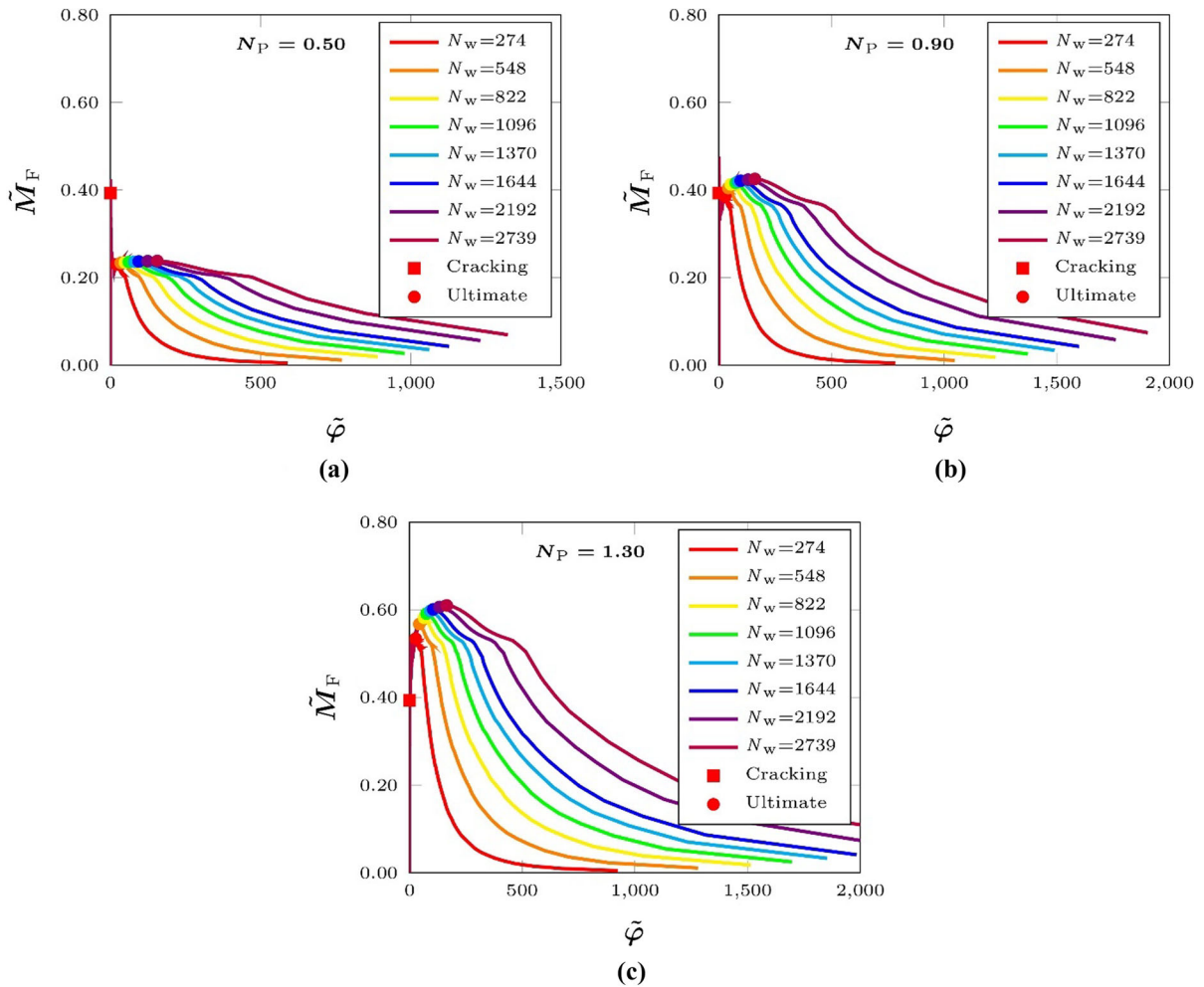


**Fig. 6** Structural response of FRC beams ( $a_0/h = 0.05$ ) as a function of  $N_w$ , and for different values of  $N_P$ : **a**  $N_P = 0.50$ ; **b**  $N_P = 0.90$ ; **c**  $N_P = 1.30$ . For each curve, the square marker

indicates the first cracking moment, whereas the circle one indicates the ultimate moment

moment,  $\tilde{M}_{cr}$ . More precisely, a decrease in  $a_0/h$  provides a nonlinear increase in  $\tilde{M}_{cr}$ , the latter tending to infinity for an unnotched specimen (LEFM). On the other hand, the initial notch depth has substantially no influence on the post-cracking regime—which is governed by  $N_P$  in Stage II and  $N_w$  in Stage III, respectively—thus leading to the same value of the load bearing capacity,  $\tilde{M}_u$ . As a consequence, considering that the stability of the flexural response is defined by  $\tilde{M}_{cr}$  and  $\tilde{M}_u$ , the numerical model predicts an increase in the critical value of the reinforcement brittleness number,  $N_{PC}$ , with a decrease in the initial notch depth,  $a_0/h$ . Further quantitative information regarding the influence of initial the notch depth on the

critical value of the reinforcement brittleness number can be found in Accornero et al. (2022a).

Regarding size-scale effects, an increase in beam depth,  $h$ , provides an increase in  $N_P$  and a decrease in  $N_w$ , consistently with Eqs. (4)–(5). Considering the numerical simulation shown above, it implies a larger stability in Stage II of the response, whereas a steeper pull-out tail (Stage III) is observed.

When the specimen size is very large, the fracture process zone—intended as the crack zone bridged by the reinforcing fibres (see Fig. 3)—becomes independent from the specimen geometry. By increasing the structural scale, the flexural response tends towards a LEFM limit condition, in which the toughening contribution of the concrete matrix and of the

reinforcing fibres can be merged together by defining an equivalent fracture toughness of the composite. On the other hand, a further limit case can be observed when the specimen size is very small: the crack propagation process is mainly governed by the concrete matrix, whose nonlinearities cannot be neglected, thus making LEFM not suitable (Massabò 2008).

#### 4 Experimental validation

In this section, UBCM is used to calibrate the model constitutive parameters on the basis of experimental results reported in the literature. After calibration, UBCM is used as a predictive tool in order to evaluate the influence of the specimen size on the stability of the FRC flexural response.

The experimental campaign under consideration was carried out by Jones et al. (2008), who investigated the flexural behaviour of FRC beams by means of four-point bending tests on unnotched FRC specimens characterized by a span of 500 mm, a thickness of 100 mm, and variable depths ranging from 50 to 100 mm (Fig. 7).

The composite under investigation was made of a concrete matrix characterized by a 28-days cubic compression strength of 72 MPa, reinforced with hooked-end steel fibres of 30 mm in length,  $l_f$ , aspect ratio  $\lambda_f = l_f/d_f = 60$ , and tensile strength,  $f_u = 1100$  MPa. The experimental program included: (i) two fibre contents equal to 40 kg/m<sup>3</sup> ( $V_f = 0.50\%$ ) and 80 kg/m<sup>3</sup> ( $V_f = 1.00\%$ ); (ii) three different specimen depths as depicted in Fig. 7.

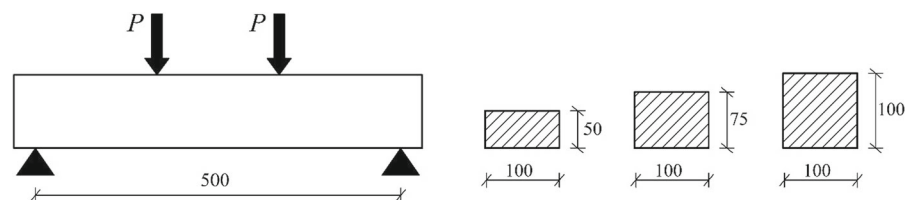
For each combination of fibre volume fraction and specimen size, three specimens were tested in four-point bending. Further information about the composition and the mechanical properties of the composite mixture can be found in Jones et al. (2008).

#### 4.1 Identification procedure

The numerical modelling has been carried out by considering the reinforcing layers evenly spaced within the ligament area. Since no information regarding the fibre distribution are available from the considered experimental tests, the orientation factor,  $\alpha$ , is assumed equal to one. The same assumption was applied for the coefficient  $\beta_i$ . Nevertheless, these assumptions do not limit the application of the model because, as explained above, they are included in the equivalent slippage strength,  $\tilde{\sigma}_{s,max}$ , which can be identified on the basis of the experimental curves. Then, the bridging law represented in Fig. 4b has been adopted for the analysis, since hooked-end steel fibres are used in the experimental investigation. Finally, a fictitious initial notch of depth  $a_0/h = 0.05$  has been used to model the initially smooth specimen. The influence of this choice on the obtained results will be discussed later in this section.

For each of the six specimen series, three experimental curves are averaged in order to obtain the corresponding load vs mid-span deflection diagram. Then, an identification procedure has been applied in order to identify the mechanical parameters of the matrix and of the reinforcing fibres, i.e.,  $K_{IC}$ ,  $\tilde{\sigma}_{s,max}$ , and  $w_c$ , which cannot be known a priori. The matrix fracture toughness,  $K_{IC}$ , is determined as the first parameter, being related to the first cracking moment of the FRC specimen. In other words,  $K_{IC}$  is found by optimizing the difference between the first cracking moment experienced by the specimen and that predicted by the numerical model. On the other hand, the other two parameters,  $\tilde{\sigma}_{s,max}$  and  $w_c$ , relate to the post-cracking behaviour of the composite, being directly related to the abovementioned dimensionless numbers,  $N_p$  and  $N_w$ . In this case,  $\tilde{\sigma}_{s,max}$  and  $w_c$  have been selected by taking into account two parameters: the maximum load, i.e., the load-bearing capacity of the specimen, and the area under the load vs deflection curve. For each pair of values ( $\tilde{\sigma}_{s,max}$ ,  $w_c$ ), the

**Fig. 7** Test geometry adopted in Jones et al. (2008)



comparison between a given experimental curve and the related numerical prediction permits the evaluation of the differences in terms of maximum load ( $\Delta P_{\max}$ ) and of the area under the curve ( $\Delta Area$ ), as schematically shown in Fig. 8a.

The problem consists in the optimization of multiple objectives by varying a set of multiple parameters. It can be addressed by applying the Pareto's approach for the multi-objective optimization. Following this route, the objective functions are  $\Delta P_{\max}$  and  $\Delta Area$ , which need to be minimized in order to find the best overlap between the experimental curve and the numerical prediction. On the other hand, the variable parameters are  $\tilde{\sigma}_{s,\max}$  and  $w_c$ , which must satisfy the following constraining conditions:  $\tilde{\sigma}_{s,\max}$  must be greater than zero, whereas  $w_c$  must be included between zero and half fibre length.

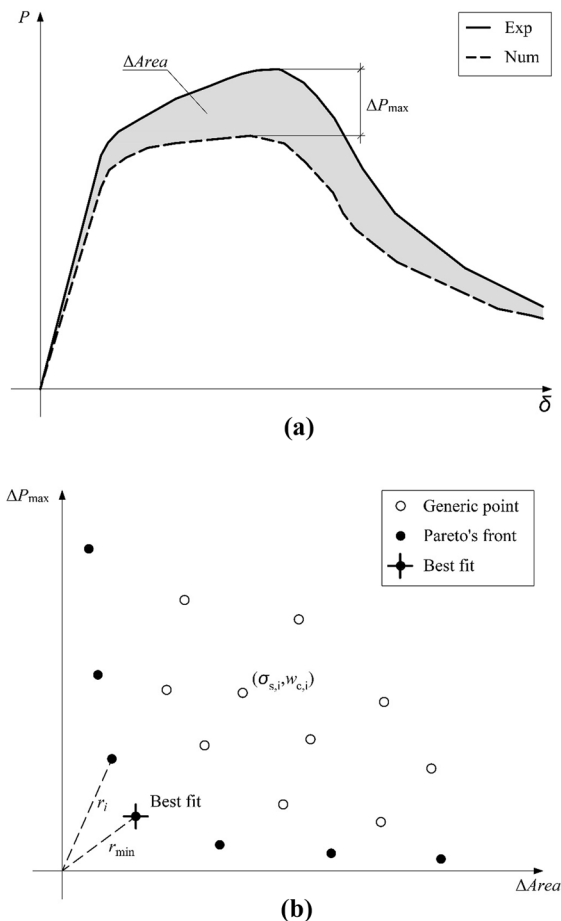


**Fig. 8** **a** Schematic representation of  $\Delta P_{\max}$  and  $\Delta Area$ ; **b** multi-objective optimization following the Pareto's procedure

Within these boundary conditions, each pair of values  $(\tilde{\sigma}_{s,\max}, w_c)$  constitutes an acceptable solution, leading to the corresponding values of the two objective functions,  $\Delta Area$  and  $\Delta P_{\max}$ . This solution can be represented by a point in the plane  $(\Delta Area, \Delta P_{\max})$  (Fig. 8a). A solution is said to be “Pareto efficient” if there is no variation able to produce improvements in one objective function, without deteriorating the other one. All the Pareto efficient solutions constitute the set of the Pareto's front (marked black points in Fig. 8b). In this application, the best-fitting solution has been chosen among the points within the Pareto's front as the one with the minimum distance from the origin (Fig. 8b).

Following this route, it is possible to obtain the set of three identifying parameters ( $K_{IC}$ ,  $\tilde{\sigma}_{s,\max}$ ,  $w_c$ ) for each specimen series, which are summarized in Table 1. The corresponding results are represented in Fig. 9 where, for each specimen series, the experimental curve is depicted together with the corresponding numerical one.

Considering the identified parameters collected in Table 1, it is worth noting that, in the case of small specimens, the matrix fracture toughness,  $K_{IC}$ , is found to be significantly smaller than that obtained in the other two cases (medium and large specimen). This result, which appears unexpected at first sight, finds a clear explanation in the framework of Fracture Mechanics. In fact, by reducing the specimen size, a transition from a crack propagation collapse, typical of LEFM, to a plastic flow collapse at the concrete ligament occurs. Consistently with the previous discussions, UBCM cannot capture this further transition, which actually requires a cohesive-crack modelling.

On the basis of these considerations, the results obtained in the case of the smallest specimens ( $h = 50$  mm) have not been considered for the identification of the mechanical properties of the composite, which are now calculated by averaging the results obtained in the case of the medium and large specimens (see Table 2).

#### 4.2 Prediction of scale effects

When the mechanical properties of the composite are obtained, the UBCM can be used as a predictive tool, and the influence of the specimen size on the flexural

**Table 1** Mechanical parameters obtained by identification

ID	$V_f$ (%)	$K_{IC}$ (MPa mm <sup>1/2</sup> )	$\tilde{\sigma}_{s,max}$ (MPa)	$w_c$ (mm)
50C (40)	0.50	14	292	9.6
75C (40)	0.50	21	359	9.6
100C (40)	0.50	23	351	11.1
50C (80)	1.00	18	273	6.9
75C (80)	1.00	23	290	8.7
100C (80)	1.00	25	283	9.0

**Fig. 9** Identification of the experimental curves:  
**a**  $V_f = 0.50\%$  (40 kg/m<sup>3</sup>);  
**b**  $V_f = 1.00\%$  (80 kg/m<sup>3</sup>)

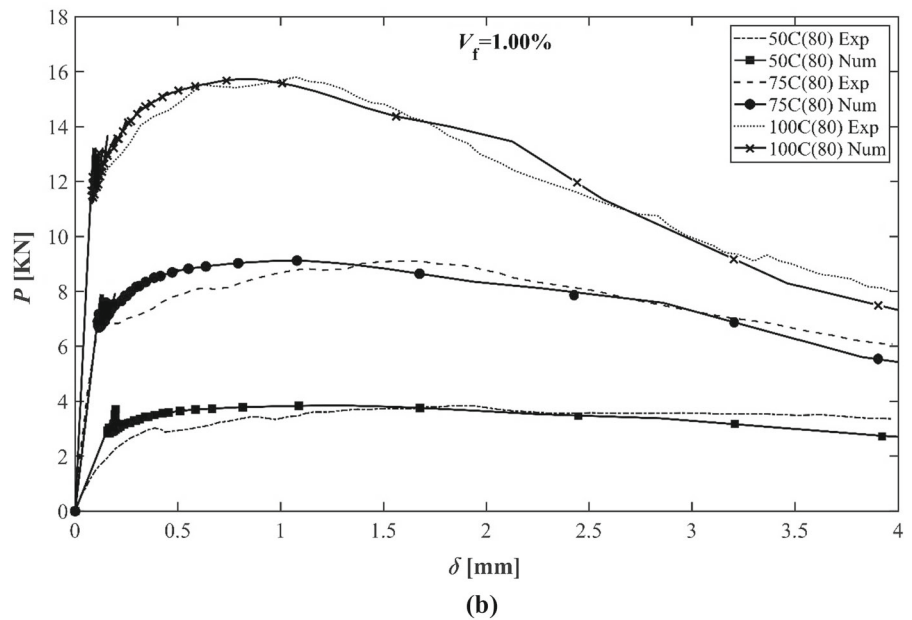
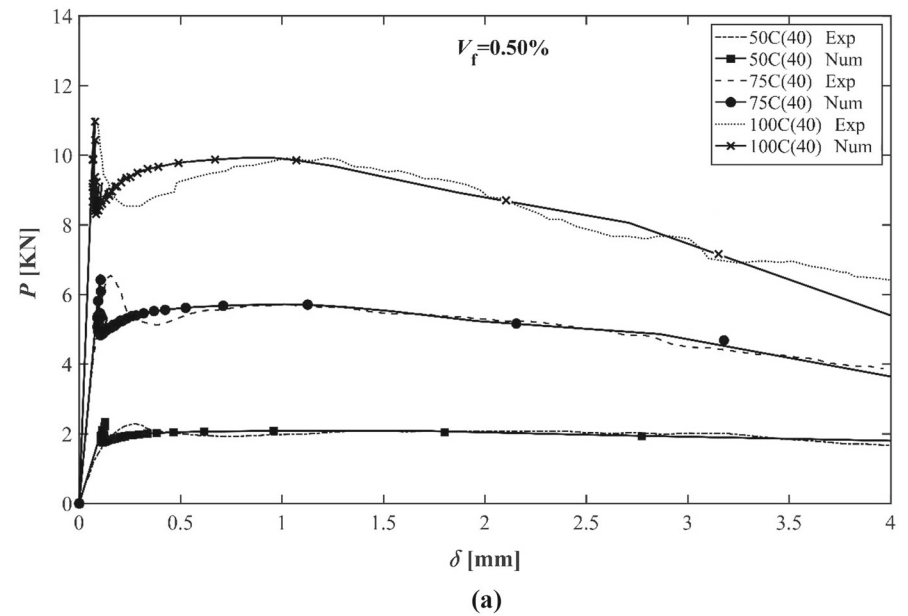


**Table 2** Average mechanical parameters used to predict size effects

ID	$V_f$ (%)	$K_{IC}$ (MPa mm <sup>1/2</sup> )	$\bar{\sigma}_{s,max}$ (MPa)	$w_c$ (mm)
75C (40)	0.50	21	359	9.6
100C (40)	0.50	23	351	11.1
Average (40)	0.50	22	355	10.35
75C (80)	1.00	23	290	8.7
100C (80)	1.00	25	283	9.0
Average (80)	1.00	24	286.5	8.85

response can be investigated by varying the beam depth,  $h$ , as the unique variable.

For each fibre volume fraction, numerical predictions were performed by varying solely the structural size in order to isolate the effect of the beam depth,  $h$ , and then they have been compared to the corresponding experimental curves. As shown in Fig. 10a and b, the model is able to fully capture the post-cracking response of the composite, which is ruled by  $N_P$  and  $N_w$  (Table 3). It is worth noting that, in the case of  $V_f = 0.50\%$  (40 kg/m<sup>3</sup>),  $N_P$  increases from 0.70 to 0.81, but still remains lower than its critical value ( $N_{PC} = 0.83$  for  $a_0/h = 0.05$ ), leading to a global softening response. On the other hand, in the case of  $V_f = 1.00\%$  (80 kg/m<sup>3</sup>),  $N_P$  increases from 1.03 to 1.19, and in all cases is greater than  $N_{PC}$ , consistently with the observed pseudo-hardening behaviour of the FRC specimens.

In both cases, the prediction of the critical condition, i.e., the critical scale,  $h_{min}$ , corresponding to a stable post-cracking response, can be provided.

For  $V_f = 0.50\%$  (40 kg/m<sup>3</sup>):

$$h_{min} = \left[ N_{PC}(a_0/h) \frac{K_{IC}}{V_f \bar{\sigma}_{s,max}} \right]^2 = \left[ 0.83 \frac{22}{(0.50\%)355} \right]^2 = 106 \text{ mm.} \quad (6)$$

For  $V_f = 1.00\%$  (80 kg/m<sup>3</sup>):

$$h_{min} = \left[ N_{PC}(a_0/h) \frac{K_{IC}}{V_f \bar{\sigma}_{s,max}} \right]^2 = \left[ 0.83 \frac{24}{(1.00\%)286.5} \right]^2 = 48 \text{ mm.} \quad (7)$$

In the former case ( $V_f = 0.50\%$ ), the estimation of  $h_{min}$  is effective, whereas in the latter case ( $V_f = 1.00\%$ ),  $h_{min}$  approaches the range in which LEFM was found not suitable. It implies that, when  $N_{PC}$  is characterised by high fibre volume fractions and very small

structural sizes, the definition of  $h_{min}$  requires further investigations.

It is worth noting that the value of  $h_{min}$  depends on the mechanical parameters of the composite and on the critical value of the reinforcement brittleness number,  $N_{PC}$ , which in turn are affected by the choice of  $a_0/h$  that is required to model a nominally unnotched specimen. In this work, it has been assumed  $a_0 = 0.05 h$ .

As explained above, the initial crack depth mainly affects the value of the first cracking moment, whereas it has little influence on the post-cracking regime of the structural response. As a consequence,  $a_0/h$  affects the identification of  $K_{IC}$ , rather than that of the fibre constitutive parameters,  $\bar{\sigma}_{s,max}$  and  $w_c$ . The correct value of the first cracking moment can be captured by means of different combinations of  $a_0/h$  and  $K_{IC}$ : an increase in  $a_0/h$  provides an increment in  $K_{IC}$ . On the other hand, an increase in  $a_0/h$  provides a decrease in  $N_{PC}$ , as previously pointed out.

Therefore, different assumptions of  $a_0/h$  lead to different values of  $K_{IC}$  and  $N_{PC}$ , although it can be shown that their product remains unchanged, leading to the same prediction in terms of critical structural size,  $h_{min}$  (see Eqs. 6, 7).

In conclusion, the key-point of the discussion is that, within the limit of applicability of LEFM, a consistent evaluation of the mechanical properties of the composite (by means of the identification procedure) leads to define the specimen size corresponding to the critical condition ( $N_P = N_{PC}$ ). This is analogous to the determination of the minimum fibre volume fraction of the composite (Carpinteri and Accornero 2020),  $V_{f,min}$ , being both  $V_f$  and  $h$  involved in the reinforcement brittleness number,  $N_P$ .

**Fig. 10** Prediction of the experimental curves:  
**a**  $V_f = 0.50\%$  ( $40 \text{ kg/m}^3$ );  
**b**  $V_f = 1.00\%$  ( $80 \text{ kg/m}^3$ )

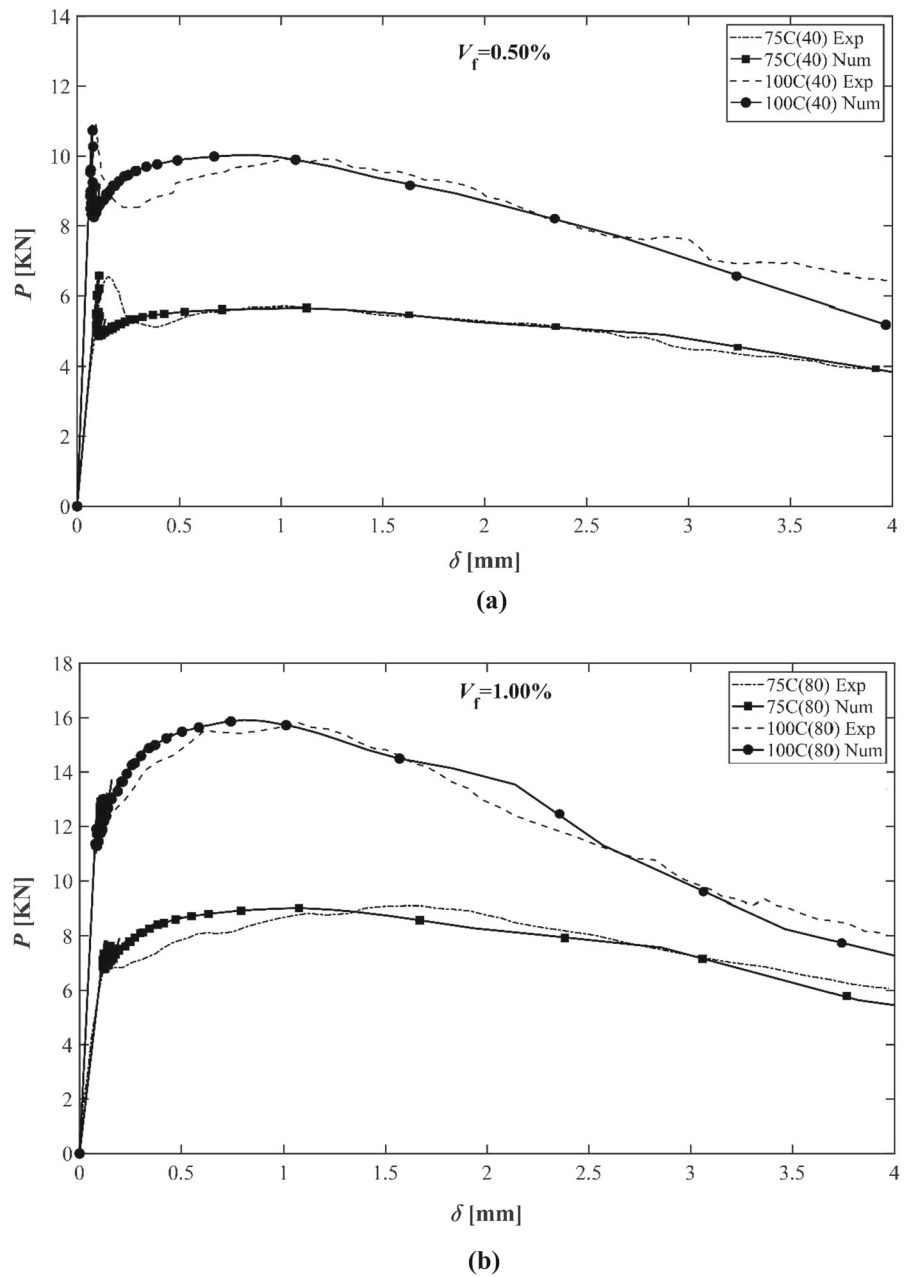


**Table 3** Brittleness numbers  $N_p$  and  $N_w$

ID	$V_f$ (%)	$K_{IC}$ (MPa mm <sup>1/2</sup> )	$\tilde{\sigma}_{s,max}$ (MPa)	$w_c$ (mm)	$h$ (mm)	$N_p$	$N_w$
75C (40)	0.50	22	355	10.35	75	0.70	2210
100C (40)	0.50	22	355	10.35	100	0.81	1914
75C (80)	1.00	24	286.5	8.85	75	1.03	1732
100C (80)	1.00	24	286.5	8.85	100	1.19	1500

## 5 Conclusions

UBCM has been proposed as a Fracture Mechanics nonlinear approach to capture and interpret the scale effects in the structural behaviour of fibre-reinforced concrete beams in bending. Within the model assumptions, the post-cracking behaviour of the composite is governed by two dimensionless numbers,  $N_P$  and  $N_w$ , which are both scale-dependent. In this respect, due to an increment in beam depth,  $h$ , a double brittle–ductile–brittle transition can be predicted. The critical value of the reinforcement brittleness number,  $N_{PC}$ , permits description of the conditions required to guarantee a stable post-peak response, both in terms of minimum fibre volume fraction or, analogously, of minimum specimen depth. Numerical predictions are compared to experimental results related to flexural tests on FRC beams of different depths. In the first step, the experimental data have been used to identify the material mechanical properties. Once the mechanical properties of the composite have been implemented (average values), UBCM has proved its potential applicability in predicting the effect of the specimen size variation on the stability of the post-cracking regime. The model allows prediction of the critical size,  $h_{min}$ , for which a stable post-peak response is obtained, analogously to the case of the minimum fibre volume fraction,  $V_{f,min}$ .

**Funding** Open access funding provided by Politecnico di Torino within the CRUI-CARE Agreement.

### Declarations

**Competing interests** The authors declare that they have no known competing financial interests or personal relationships that could have appeared to influence the work reported in this paper.

**Open Access** This article is licensed under a Creative Commons Attribution 4.0 International License, which permits use, sharing, adaptation, distribution and reproduction in any medium or format, as long as you give appropriate credit to the original author(s) and the source, provide a link to the Creative Commons licence, and indicate if changes were made. The images or other third party material in this article are included in the article's Creative Commons licence, unless indicated otherwise in a credit line to the material. If material is not included in the article's Creative Commons licence and your intended use is not permitted by statutory regulation or exceeds the permitted use, you will need to obtain permission directly from the copyright holder. To view a copy of this licence, visit <http://creativecommons.org/licenses/by/4.0/>.

## References

- Abdallah S, Rees DWA (2019) Analysis of pull-out behaviour of straight and hooked end steel fibres. *Engineering* 11(6):332–341. <https://doi.org/10.4236/eng.2019.116025>
- Abdallah S, Fan M, Rees DWA (2018) Bonding mechanisms and strength of steel fiber-reinforced cementitious composites: overview. *J Mater Civil Eng (ASCE)* 30(3):4018001. [https://doi.org/10.1061/\(ASCE\)MT.1943-5533.0002154](https://doi.org/10.1061/(ASCE)MT.1943-5533.0002154)
- Accornero F, Rubino A, Carpinteri A (2020) Ductile-to-brittle transition in fiber-reinforced concrete beams: scale and fiber volume fraction effects. *Mater Design Process Commun.* <https://doi.org/10.1002/mdp.127>
- Accornero F, Rubino A, Carpinteri A (2022) A fracture mechanics approach to the design of hybrid-reinforced concrete beams. *Eng Fract Mech.* <https://doi.org/10.1016/j.engfracmech.2022.108821>
- Accornero F, Rubino A, Carpinteri A (2022a) Post-cracking regimes in the flexural behaviour of fibre-reinforced concrete beams. *Int J Solids Struct.* <https://doi.org/10.1016/j.ijsolstr.2022.111637>
- Accornero F, Rubino A, Carpinteri A (2022b) Ultra-low cycle fatigue (ULCF) in fibre-reinforced concrete beams. *Theor Appl Fract Mech.* <https://doi.org/10.1016/j.tafmec.2022.103392>
- Almusallam T, Ibrahim SM, Al-Salloum Y, Abadel A, Abbas H (2016) Analytical and experimental investigations on the fracture behaviour of hybrid fiber reinforced concrete. *Cement Concr Compos* 74:201–217. <https://doi.org/10.1016/j.cemconcomp.2016.10.002>
- Alwan JM, Naaman AE, Guerrero P (1999) Effect of mechanical clamping on the pull-out response of hooked steel fibers embedded in cementitious matrices. *Concr Sci Eng* 1(1):15–25
- Aydin S (2013) Effects of fiber strength on fracture characteristics of normal and high strength concrete. *Period Polytech Civil Eng* 57(2):191–200. <https://doi.org/10.3311/PPci.7174>
- Barr BIG, Lee MK, de Place Hanses EJ, Dupont D, Erdem E, Schaerlaekens S, Schnutgen B, Stang H, Vandewalle L (2003) Round-robin analysis of the RILEM TC 162-TDF beam-bending test: part 1—test method evaluation. *Mater Struct* 36(10):609–620. <https://doi.org/10.1007/BF02483281>
- Barros JOA, Sena Cruz J (2001) Fracture energy of steel fiber-reinforced concrete. *Mech Compos Mater Struct* 8(1):29–45. <https://doi.org/10.1080/10759410119428>
- Barros JOA, Cunha VMCF, Ribeiro AF, Antunes JAB (2005) Post-cracking behaviour of steel fibre reinforced concrete. *Mater Struct* 38(1):47–56. <https://doi.org/10.1007/BF02480574>
- Bažant ZP (1984) Size effect in blunt fracture: concrete, rock, metal. *J Eng Mech ASCE* 110(4):518–535. [https://doi.org/10.1061/\(ASCE\)0733-9399\(1984\)110:4\(518\)](https://doi.org/10.1061/(ASCE)0733-9399(1984)110:4(518))
- Bencardino F, Rizzuti L, Spadea G, Swamy RN (2010) Experimental evaluation of fiber reinforced concrete fracture properties. *Composites B* 41(1):17–24. <https://doi.org/10.1016/j.compositesb.2009.09.002>

- Bosco C, Carpinteri A (1995) Discontinuous constitutive response of brittle matrix fibrous composites. *J Mech Phys Solids* 43(2):261–274. [https://doi.org/10.1016/0022-5096\(94\)00058-D](https://doi.org/10.1016/0022-5096(94)00058-D)
- Carpinteri A (1981) A fracture mechanics model for reinforced concrete collapse. In: Proceedings of the IABSE colloquium on advanced mechanics of reinforced concrete, Delft, pp 17–30
- Carpinteri A (1984a) Stability of fracturing process in RC beams. *J Struct Eng ASCE* 110(3):544–558. [https://doi.org/10.1061/\(ASCE\)0733-9445\(1984\)110:3\(544\)](https://doi.org/10.1061/(ASCE)0733-9445(1984)110:3(544))
- Carpinteri A (1984b) Hysteretic behavior of RC beams. *J Struct Eng ASCE* 110(9):2073–2084. [https://doi.org/10.1061/\(ASCE\)0733-9445\(1984\)110:9\(2073\)](https://doi.org/10.1061/(ASCE)0733-9445(1984)110:9(2073))
- Carpinteri A (1994) Scaling laws and renormalization groups for strength and toughness of disordered materials. *Int J Solids Struct* 31(3):291–302. [https://doi.org/10.1016/0020-7683\(94\)90107-4](https://doi.org/10.1016/0020-7683(94)90107-4)
- Carpinteri A, Accornero F (2019) The bridged crack model with multiple fibers: local instabilities, scale effects, plastic shake-down, and hysteresis. *Theoret Appl Fract Mech* 104:102351. <https://doi.org/10.1016/j.tafmec.2019.102351>
- Carpinteri A, Accornero F (2020) Residual crack opening in fiber-reinforced structural elements subjected to cyclic loading. *Strength Fract Complex* 12(2–4):63–74. <https://doi.org/10.3233/SFC-190236>
- Carpinteri A, Massabò R (1996) Bridged versus cohesive crack in the flexural behavior of brittle–matrix composites. *Int J Fract* 81(2):125–145. <https://doi.org/10.1007/BF00033178>
- Carpinteri A, Massabò R (1997a) Continuous vs discontinuous bridged crack model of fiber-reinforced materials in Flexure. *Int J Solids Struct* 34(18):2321–2338. [https://doi.org/10.1016/S0020-7683\(96\)00129-1](https://doi.org/10.1016/S0020-7683(96)00129-1)
- Carpinteri A, Massabò R (1997b) Reversal in failure scaling transition of fibrous composites. *J Eng Mech ASCE* 123(2):107–114. [https://doi.org/10.1061/\(ASCE\)0733-9399\(1997\)123:2\(107\)](https://doi.org/10.1061/(ASCE)0733-9399(1997)123:2(107))
- Carpinteri A, Puzzi S (2007) The bridged crack model for the analysis of brittle matrix fibrous composites under repeated bending loading. *J Appl Mech ASME Trans* 74(6):1239–1246. <https://doi.org/10.1115/1.2744042>
- Choi W-C, Jung K-Y, Jang S-J, Yun H-D (2019) The influence of steel fiber tensile strengths and aspect ratios on the fracture properties of high-strength concrete. *Materials* 12(13):2105. <https://doi.org/10.3390/ma12132105>
- Fantilli AP, Chiaia B, Gorino A (2016) Fiber volume fraction and ductility Index of concrete beams. *Cement Concr Compos* 65:139–149. <https://doi.org/10.1016/j.cemconcomp.2015.10.019>
- Flàdr J, Bily P (2018) Specimen size effect on compressive and flexural strength of high-strength fibre-reinforced concrete containing coarse aggregate. *Composites B* 138:77–86. <https://doi.org/10.1016/j.compositesb.2017.11.032>
- Holschemacher K, Mueller T, Ribakov Y (2010) Effect of steel fibres on mechanical properties of high-strength concrete. *Mater Des* 31(5):2604–2615. <https://doi.org/10.1016/j.matdes.2009.11.025>
- Jones PA, Austin SA, Robins PJ (2008) Predicting the flexural load-deflection response of steel fibre reinforced concrete from strain, crack-width, fibre pull-out and distribution data. *Mater Struct* 41(3):449–463. <https://doi.org/10.1617/s11527-007-9327-9>
- Li VC, Wang Y, Backer S (1990) Effect of inclining angle, bundling and surface treatment on synthetic fibre pull-out from a cement matrix. *Composites* 21(2):132–140. [https://doi.org/10.1016/0010-4361\(90\)90005-H](https://doi.org/10.1016/0010-4361(90)90005-H)
- LoMonte F, Ferrara L (2020) Tensile behaviour identification in ultra-high performance fibre reinforced cementitious composites: indirect tension tests and back analysis of flexural test results. *Mater Struct* 53:145. <https://doi.org/10.1617/s11527-020-01576-8>
- Massabò R (2013) Bridged and cohesive crack models for fracture in composite materials. In: Mechanics down under—proceedings of the 22nd international congress of theoretical and applied mechanics (ICTAM 2008), vol 2, pp 135–154. [https://doi.org/10.1007/978-94-007-5968-8\\_9](https://doi.org/10.1007/978-94-007-5968-8_9)
- Mobasher B, Bakhshi M, Barsby C (2014) Backcalculation of residual tensile strength of regular and high performance fiber reinforced concrete from flexural tests. *Constr Build Mater* 70:243–253. <https://doi.org/10.1016/j.conbuildmat.2014.07.037>
- Naaman AE (2008) High performance fiber reinforced cement composites. In: Chung DDL (ed) High-performance construction materials. Engineering materials for technological needs. World Scientific Publishing Co. Pte. Ltd, Singapore
- Paschalis SA, Lampropoulos AP (2015) Size effect on the flexural performance of ultra high performance fiber reinforced concrete (UHPRFC). In: Proceedings of the 7th RILEM workshop on High Performance Fiber Reinforced Cement Composites (HPRCC-7), Stuttgart, pp 177–184
- RILEM TC 162-TDF (2003) Test and design method for steel fibre reinforced concrete.  $\Sigma$ - $\epsilon$  design method. Final recommendation. *Mater Struct* 36(8):560–567. <https://doi.org/10.1007/BF02480834>
- Robins P, Austin S, Jones P (2002) Pull-out behaviour of hooked steel fibres. *Mater Struct* 35:434–442. <https://doi.org/10.1007/BF02483148>
- Robins P, Austin S, Jones P (2003) Spatial distribution of steel fibres in sprayed and cast concrete. *Mag Concr Res* 55(3):225–235. <https://doi.org/10.1680/MACR.2003.55.3.225>
- Rubino A, Accornero F, Carpinteri A (2021) Post-cracking structural behaviour in FRC beams: Scale effects and minimum fibre volume fraction. Proceedings of the FIB Symposium 2021, Lisbon, Portugal, pp 622–631
- Sahin Y, Koksall F (2011) The influences of matrix and steel fibre tensile strengths on the fracture energy of high-strength concrete. *Constr Build Mater* 25(4):1801–1806. <https://doi.org/10.1016/j.conbuildmat.2010.11.084>
- Soetens T, Matthys S (2014) Different methods to model the post-cracking behaviour of hooked-end steel fibre reinforced concrete. *Constr Build Mater* 73:458–471. <https://doi.org/10.1016/j.conbuildmat.2014.09.093>
- Yoo D-Y, Yoon Y-S, Banthia N (2015) Flexural response of steel-fibre-reinforced concrete beams: effects of strength fiber content, and strain-rate. *Cement Concr Compos* 64:84–92. <https://doi.org/10.1016/j.cemconcomp.2015.10.001>
- Yoo D-Y, Banthia N, Yang Y, Yoon Y-S (2016) Size effect in normal- and high-strength amorphous metallic and steel



fiber reinforced concrete beams. *Constr Build Mater* 121:676. <https://doi.org/10.1016/j.conbuildmat.2016.06.040>

**Publisher's Note** Springer Nature remains neutral with regard to jurisdictional claims in published maps and institutional affiliations.